Parameterized attenuated exchange for generalized TDHF@v_w applications ⊘

Barry Y. Li ✉ Ⓘ ; Tim Duong Ⓘ ; Tucker Allen Ⓘ ; Nadine C. Bradbury Ⓘ ; Justin R. Caram Ⓘ ;
Daniel Neuhauser Ⓘ

[Check for updates]

⊡ CHORUS

View Online   Export Citation

Articles You May Be Interested In

Density fitting in periodic systems: Application to TDHF in diamond and oxides

J. Chem. Phys. (August 2020)

Photoionization and core resonances from range-separated density-functional theory: General formalism and example of the beryllium atom

J. Chem. Phys. (June 2022)

Short-time Fourier transform analysis of real-time time-dependent Hartree–Fock and time-dependent density functional theory calculations with Gaussian basis functions
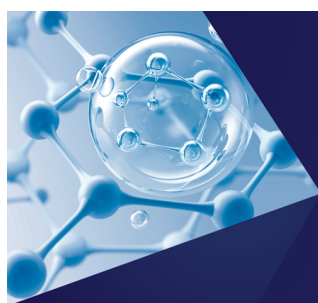
J. Chem. Phys. (February 2010)

Parameterized attenuated exchange for generalized TDHF@v_W applications

View Online   Export Citation   CrossMark

Barry Y. Li,[1,a] (iD) Tim Duong,[1] (iD) Tucker Allen,[1] (iD) Nadine C. Bradbury,[2] (iD) Justin R. Caram,[1,b] (iD) and Daniel Neuhauser[1,c] (iD)

AFFILIATIONS

[1] Department of Chemistry and Biochemistry, University of California, Los Angeles, Los Angeles, California 90095, USA

[2] Department of Chemistry, Princeton University, Princeton, New Jersey 08544, USA

Note: This paper is part of the JCP Special Topic, Festschrift for Abraham Nitzan.
a) Author to whom correspondence should be addressed: barryyangtao@chem.ucla.edu
b) jcaram@chem.ucla.edu
c) dxn@ucla.edu

ABSTRACT

Building upon our previously developed time-dependent Hartree–Fock (TDHF)@v_W method, based on many-body perturbation theory and, specifically, the Bethe–Salpeter Equation (BSE), we introduce a parameterization scheme for the attenuated exchange kernel, $v_W(|r - r'|)$. In the original method, v_W was determined individually for each system via an efficient stochastic short-time TD Hartree propagation for the screened Coulomb interaction, $W(r, r')$. The new parameterization leverages photophysical similarities in exciton binding energies (or exchange interaction attenuation) among molecules with comparable static dielectric responses. We parameterize the inverse dielectric function using a low-order polynomial with error function apodization, calibrated on a few representative molecules, each with its own v_W. Using only seven parameters, the parameterized v_W is fully grid-independent and broadly applicable within a family of molecules. This enables TDHF@v_W that retains BSE-level accuracy, achieving a mean absolute error of ~0.1 eV compared to experimental optical gaps and representing a five- to tenfold improvement over conventional TD density functional theory or TDHF while reducing the cost to that of standard TDHF.

Published under an exclusive license by AIP Publishing. https://doi.org/10.1063/5.0273771

I. INTRODUCTION

The GW-Bethe–Salpeter equation (GW-BSE) approach has become a very popular method to accurately calculate the optical absorption spectra of molecular systems. Within the framework of many-body perturbation theory (MBPT), the success of the method lies in the explicit inclusion of an effective screened Coulomb interaction kernel, W.[1,2] An improved description of electron correlation through W makes the GW-BSE method capable of capturing the complex multi-configurational character of excited states, such as those present in delocalized, highly conjugated molecular systems with closely spaced energy levels that are not well described by time-dependent density functional theory (TDDFT).[3–5]

Employing the static and Tamm–Dancoff approximations, the BSE describes couplings of singlet electron–hole pairs, i.e., excitons, through the resonant matrix, A,

$$A_{ia,jb} = (\varepsilon_a - \varepsilon_i + \Delta)\delta_{ij}\delta_{ab} + 2(ia|jb) - (ab|W|ij), \quad (1)$$

where the $N_v N_c \times N_v N_c$ valence–conduction product basis is composed of a generalized Kohn–Sham DFT eigensystem. Indices $i, j, \dots$ refer to valence (hole) states, and $a, b, \dots$ refer to conduction (electron) states. A GW-derived scissor energy correction, Δ, is then applied to the independent-particle term of A to include single-particle self-energy effects.[6,7] Assuming real orbitals, the bare Coulomb integrals are

$$(ia|jb) = \int dr\, dr'\, \phi_i(r)\phi_a(r)|r - r'|^{-1}\phi_j(r')\phi_b(r') \quad (2)$$

and the screened direct interaction matrix elements are

$$(ab|W|ij) = \int dr\, dr'\, \phi_a(r)\phi_b(r)W(r, r')\phi_i(r')\phi_j(r'). \quad (3)$$

Replacing the effective interaction, $W(r, r')$, with the bare Coulomb potential, $|r - r'|^{-1}$, and letting $\Delta = 0$ (i.e., not requiring a separate GW calculation on the HOMO and LUMO levels) converts Eq. (1) to the Casida formulation of time-dependent Hartree–Fock (TDHF).[8] Following the frequency-domain approach of Ref. 9, this is equivalent to the random phase approximation with exchange (RPA-X) of quantum chemistry.

Constructing and storing the matrix elements of Eq. (3) becomes the major computational bottleneck of a BSE calculation with an overall scaling of $\mathcal{O}(N^4)$. It is standard practice to obtain $W(r, r')$ within the RPA.[10] In the frequency domain, this requires evaluating the static limit of the full dielectric matrix, $\epsilon(r, r'')$, whose inverse relates to W by

$$W(r, r') = \int dr'' \epsilon^{-1}(r, r'') |r'' - r'|^{-1}. \tag{4}$$

Meanwhile, in the time-domain, the elements of Eq. (3) are obtained through a time-dependent Hartree (TDH) propagation by perturbing and propagating all occupied states.[11]

We have shown in several previous works that efficient stochastic techniques can enable GW-BSE calculations for systems consisting of hundreds to thousands of valence electrons. This includes an exact division of W to simpler terms, $W \equiv v_W + \{W - v_W\}$, where $v_W(|r - r'|)$ is a momentum-space diagonal (i.e., translationally invariant) attenuated exchange kernel that captures the bulk of the effect of W and $\{W - v_W\}$ is the remaining difference that is stochastically sampled.[6,7,12,13]

The methodology is detailed in Refs. 6, 9, and 14 and summarized here. We wish to approximate the effect of $W(r, r')$ on occupied–occupied pair densities by minimizing the objective $\sum_{ij} (ij|(W - v_W)^2|ij)$ to obtain a simpler screened exchange kernel, v_W. First, a set of statistically independent stochastic occupied orbitals is introduced, $\bar{\beta}(r) = \sum_i (\pm 1) \phi_i(r)$ and $\bar{\bar{\beta}}(r) = \sum_i (\pm 1) \phi_i(r)$, which yield a pair density $\beta(r) \equiv \bar{\beta}(r) \bar{\bar{\beta}}(r)$. With a few manipulations, the optimal form of v_W is expressed in reciprocal space,

$$v_W(k) = \left\{ \frac{\beta^*(k) \langle k|W|\beta \rangle}{|\langle k|\beta \rangle|^2} \right\}_\beta, \tag{5}$$

where $\{\cdots\}$ indicates a statistical average over the number of stochastic samples, β. The action of the many-body W on a random pair density, $W_\beta(k) \equiv \langle k|W|\beta \rangle$, is obtained in real-space through a stochastic TDH propagation with a source potential derived from $\beta(r)$. As verified in our previous studies, typically 2000 stochastic samples are sufficient for convergence of both v_W and the BSE absorption spectrum.[6,14]

The TDHF@v_W method is obtained by replacing W with v_W for the electron–hole interaction kernel, omitting the difference, $\{W - v_W\}$.[6] In our recent work, we applied this method to several π-conjugated, near- and shortwave-infrared dyes, including the flavylium (Flav) and indocyanine green (ICG) families of polymethine cyanine dyes (molecular structures shown in Fig. 1), and demonstrated good agreement between the calculated spectra and experimental measurements.[14]

The computational scheme was detailed in our previous publication, Ref. 14. Figure 2(a) summarizes the procedure: the (semi)local density approximation (LDA) DFT is performed first,
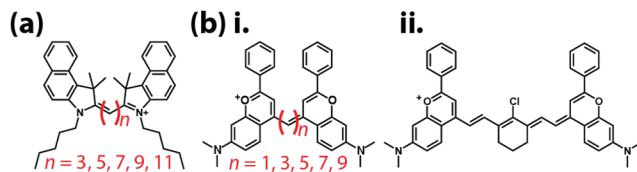

FIG. 1. (a) ICG dye structures with various polymethine chain lengths. (b-i) Flav dye structures, where $n = 7$ means LFlav-7 (the linear Flav-7); (b-ii) Flav-7.[14]

followed by a near-gap hybrid treatment to include explicit exchange.[9,13] Next, a small number of stochastic actions, W_β, yield the static RPA response,[12] where v_W is then individually fitted by averaging over W_β, per Eq. (5).[6,14] Finally, v_W is used as an attenuated exchange kernel in the TDHF calculations for optical spectra.

We observed that the individually fitted v_W are similar among these dyes [Fig. 2(b)], indicating that there exists a generalized, parameterizable form of the exchange kernel for families of molecules with similar dielectric screening. Thus, we can bypass the need of W_β and the individually fitted v_W as indicated by the green path [Fig. 2(a)]. Reducing the computational cost to conventional TDHF while maintaining BSE-quality results is a long-standing goal.[15] Here, we introduce a parameterization scheme [Fig. 2(c)] of v_W, allowing for the use of a single kernel at the TDHF level for various molecules regardless of the system or computational grid. We also provide a simple functional form of v_W for families of
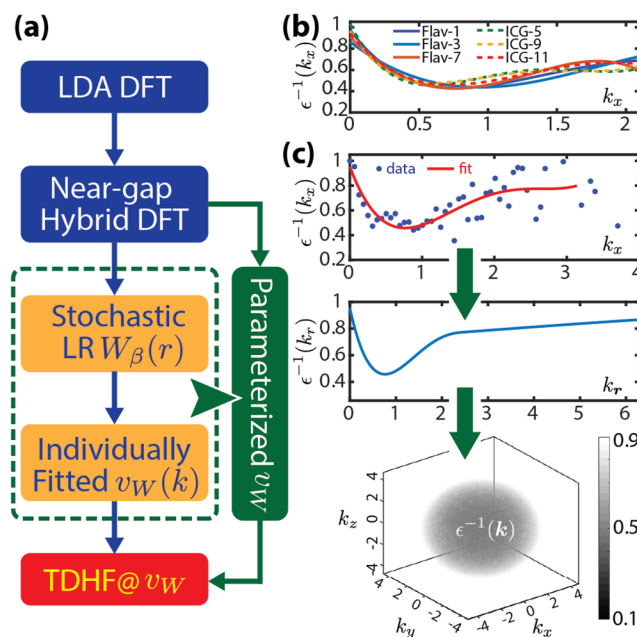

FIG. 2. (a) Schematic flow of the overall computation. The parameterization (in green) of v_W in this work replaces the needs of individual stochastic linear-response W_β and v_W generation. (b) $\epsilon^{-1}(k)$ for a few Flav and ICG dyes.[14] (c) Schematic $\epsilon^{-1}(k)$ parameterization and regeneration process.

molecules, avoiding the need to prepare the stochastic actions W_β altogether.

Section II describes our parameterization procedure and demonstrates its application through three sets of parameterized results for different molecular families: 11 polymethine cyanine dyes, six planar aromatic hydrocarbons, and three curved aromatic hydrocarbons (structures in Fig. 1 and Appendix A). All molecular geometries are optimized under vacuum using ORCA 6.0 at the B3LYP/def2-TZVPPD level.[16,17] All geometries were optimized with ORCA's B3LYP (distinct from Gaussian's B3LYP/G) for consistency with Ref. 14. With our generalized, parameterized, functional form of v_W, the TDHF@v_W formalism can be made even cheaper with a balance between computational complexity (at the cost of TDHF) and accuracy (at the near-BSE quality) for optical excitation spectra. By doing so, we unlock the full potential to elucidate photophysical properties for various classes of chromophores, improving their application in fluorescence detection techniques and the study of larger biomolecules through a simple, generalized parameterization of small molecules.

II. METHODOLOGY

We introduce a parameterization of $v_W(k)$ for families of molecules sharing similar static dielectric properties. The inverse dielectric function can be written as

$$\epsilon^{-1}(k) = \frac{v_W}{v_{\text{bare}}} + 1, \tag{6}$$

where $v_{\text{bare}} = |r - r'|^{-1}$. Our previous article presents $\epsilon^{-1}(k)$ for multiple Flav and ICG dyes,[14] where we realize that they reveal a striking similarity. This suggests the possibility of a generalized v_W.

Starting with a small- to mid-sized dye or hydrocarbon and performing the original stochastic fitting to extract $v_W(k)$, we proceed with a one-dimensional (1D) functional fitting of the inverse dielectric function, $\epsilon^{-1}(k_x)$, using a fourth-order polynomial,

$$f_1^x(k) = 1 + \sum_{n=0}^{4} c_n^x k^n. \tag{7}$$

We fit $\epsilon^{-1}(k_y)$ and $\epsilon^{-1}(k_z)$ with the same procedure, where k_x, k_y, and k_z are slices along the respective (1,0,0), (0,1,0), and (0,0,1) directions. To get an isotropic-averaged set of polynomial coefficients,

$$c_n = \frac{1}{3}\left(c_n^x + c_n^y + c_n^z\right), \tag{8}$$

which are used to calculate an overall f_1.

We then introduce an error function tail to handle high-k stochastic noise present due to the Martyna–Tuckerman technique used to avoid grid-reflection effects when generating the stochastic actions, W_β.[18] We define a high-k noise cutoff, k_{mt}, and the corresponding fitted function value, $f_{\text{mt}} = f_1(k_{\text{mt}})$. For $k \leq k_{\text{mt}}$, $f_1(k)$ is used. For $k > k_{\text{mt}}$,

$$f_2(k) = (2 - 2f_{\text{mt}})\left\{\frac{1}{2}\text{erf}[\gamma(k - k_{\text{mt}})] + \frac{1}{2}\right\} + 2f_{\text{mt}} - 1 \tag{9}$$

is used. Thus, the final fitted $\epsilon^{-1}(k)$ is

$$\epsilon^{-1}(k) = \begin{cases} f_1(k) & \text{for } k \leq k_{\text{mt}}, \\ f_2(k) & \text{for } k > k_{\text{mt}}. \end{cases} \tag{10}$$

We have verified with the pyrene molecule that the results are mostly insensitive to the momentum cutoff parameter k_{mt} (see Appendix B): varying k_{mt} from 1.0 to 1.5 bohr^{-1} (real-space 1.66–1.11 Å) shifts the singlet-excitation (S_1) peak by less than 4 meV. The 1D parameterization results in seven parameters: five polynomial coefficients, c_n, the noise cutoff, k_{mt}, and the steepness of the error function tail, γ. Now, everything is made off-grid and easy to store, modify, and share. It is straightforward to place the parameterized 1D function back on any customizable three-dimensional grid for application via a central-symmetric extrapolation of $\epsilon^{-1}(k)$ onto $\epsilon^{-1}(k_r)$, where $k_r = \sqrt{k_x^2 + k_y^2 + k_z^2}$.

III. RESULTS AND DISCUSSION

Plane-wave (PW) pseudopotential LDA-DFT simulations are performed for all 20 test systems, followed by a near-gap hybrid DFT calculation via the CAM-LDA0 functional to include explicit exact-exchange. The computational grid and the numbers of valence (N_v) and conduction (N_c) near-gap MOs used in the near-gap hybrid DFT step for each system are tabulated in Appendix C. Uniform grids are used for all calculations, where $dx = dy = dz \sim 0.5$ bohr with verified convergence in previous publications. For both LDA and near-gap hybrid DFT, we require the self-consistent field (SCF) energy to converge to 10^{-8} eV. For convergence of the S_1 excitation energies, we include ~5 times more unoccupied states than occupied states in the LDA-DFT stage. For exchange energy convergence, we use all occupied MOs and ~3 times more unoccupied MOs ($N_c \approx 3N_v = 3N_{\text{occ}}$) in the near-gap step. Previous work[22] has shown that a hybrid-DFT eigensystem can serve as an excellent starting point for excited-state calculations. We chose the CAM-LDA0 functional as it is well-suited for π-conjugated systems with a balanced treatment of short- and long-range exchange,[23] which effectively captures mid-range screening, a critical factor in exciton binding. As demonstrated in Ref. 14, this approach yields excitation energies in good agreement with experimental results.

All optical absorption spectra are calculated with an iterative Chebyshev solver, as in Refs. 6, 9, 12, and 14. The spectral widths of the absorption lines are determined by the number of polynomials used in the Chebyshev expansion, which is fixed at 3000 terms for all simulations. We go beyond the Tamm–Dancoff approximation for all spectral calculations, including the resonant–antiresonant coupling effects between positive- and negative-frequency transitions.[24] This is at a minimal additional cost as we implement sparse-stochastic sampling of the exchange kernel matrix elements.

Three reference molecules that represent families of molecules are chosen to generate the individually fitted v_W exchange kernel: pyrene for planar hydrocarbons, corannulene ($C_{20}H_{10}$) for curved hydrocarbons, and Flav-9 for polymethine dyes (ICG and Flav). The reference choice can be arbitrary, but we select these three due to their moderate size, good geometry convergence. Figure 3 shows the resulting spectra for these three references. The HOMO and LUMO densities are obtained from the near-gap DFT calculation using the CAM-LDA0 functional.[14,23,25,26] As expected, they are all π and π^* electronic structures and contribute predominantly to the
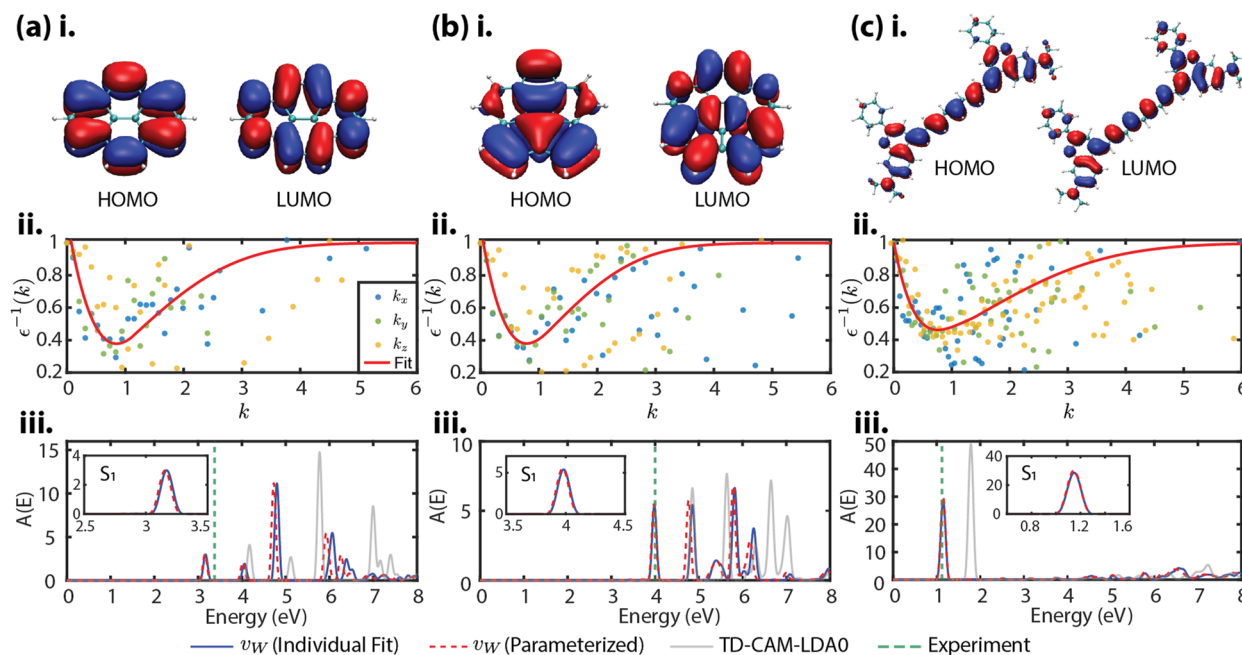
FIG. 3. For (a) pyrene, (b) corannulene, and (c) Flav-9, we show (i) the HOMO and LUMO densities calculated from near-gap hybrid DFT via the CAM-LDA0 functional; (ii) $\epsilon^{-1}(k)$ along (1,0,0), (0,1,0), and (0,0,1) directions (dots) (k is in unit of bohr^{-1}, and the parameterization is in red lines); and (iii) optical spectra calculated against the experimental S_1 energy via the individually fitted v_W, parameterized v_W, and TDDFT@CAM-LDA0. The experimental data are obtained from Refs. 19–21.

lowest singlet (S_1) excitation. Such delocalized frontier MOs require sophisticated treatment of non-local exchange over all ranges. We verified in previous work that the mid-range screening plays a crucial role in these systems for capturing correct dielectric response and exciton bindings.[14]

We also show in Fig. 3 $\epsilon^{-1}(k)$ along the x, y, and z directions overlaid by the isotropic-averaged fitting result. TDHF@v_W spectra via the individually fitted and the parameterized v_W are plotted together with the experimental S_1 peaks. The functional model with a fourth-order polynomial and an error function tail fits well in all three cases. The real-space representations of the inverse dielectric function, $\epsilon^{-1}(|r - r'|)$, for three molecules are shown in Appendix D. It is clear to see that the mid-range (0.5–2.5 Å) screening is significant for all of them, where the z-direction has a stronger screening effect than x and y because there are no adjacent atoms in the z-direction. Thus, electrons are more easily polarized by an external field along this direction. The S_1 peaks calculated for the three reference molecules from the parameterized v_W match the ones obtained from the individually fitted v_W to an accuracy of 0.01 eV (Fig. 3). The resulting parameters are tabulated in Table I.

Table II shows the S_1 peak calculated from various TDDFT and TDHF methods for two families of molecules (six Flav dyes and six planar hydrocarbons). Pure LDA has no explicit exchange, and bare HF has no electron correlation. Common hybrid-exchange functionals do not carefully treat the mid-range screening in the exchange.[4] Therefore, their mean-absolute errors (MAEs) range between ~0.3 and 1 eV for both families. MBPT-based methods, i.e.,

the v_W approach, significantly enhance the accuracy by pushing the MAE down to ~0.1 eV or below. We show TDHF@v_W results from both the individually fitted and parameterized v_W. Note that we use the parameters obtained from Flav-9 for Flav dyes and the parameters of pyrene for planar hydrocarbons. The parameterized v_W gives slightly better MAE than the individually fitted one because the functional parameterization cancels out the stochastic noise. The resulting $\epsilon^{-1}(k)$ and the corresponding v_W are smooth, which is a benefit of the present approach. We attribute the improved results for the parameterized v_W vs the individually fit v_W shown in Table II to the removal of the high-k noise in the parameterized fit given by Eq. (9).

Figure 4 shows the S_1 peaks for (a) five ICG dyes and (b) three curved hydrocarbons ($C_{20}H_{10}$, C_{60}, and [10]CPP-C_{60}) against the

TABLE I. Resulting sets of the seven fitted parameters of $\epsilon^{-1}(k)$ for pyrene, corannulene, and Flav-9.

	Pyrene	Corannulene	Flav-9
c_0	0.06	0.09	0.24
c_1	−0.63	−0.76	−1.23
c_2	2.00	2.19	2.39
c_3	−2.20	−2.21	−1.93
c_4	0.15	0.10	0.01
k_{mt}	1.10	1.20	1.40
γ	0.50	0.60	0.40

TABLE II. S_1 excitation energies (eV) of the Flav dye family (six dyes) and six planar hydrocarbons calculated using different TDDFT functionals, the individually fitted v_W, and the parameterized v_W against experimental data.[19,21,27–32] TD-LDA, TD-CAM-LDA0, and TDHF@v_W are performed with in-house grid-based codes, while the others are done in ORCA 6.0 with a def2-TZVPPD basis.[16,17] The mean-absolute error (MAE) reference to the experiments are shown for both sets.

System	LDA	PBE0	B3LYP	LC-PBE	ωB97X	CAM-LDA0	TDHF	v_W ind.	v_W par.	Expt.
Flav-1	2.04	2.54	2.47	2.88	2.81	3.29	2.53	1.73	1.78	1.90[21]
Flav-3	2.05	2.45	2.41	2.56	2.52	2.39	2.92	1.62	1.65	1.66[21]
Flav-5	1.97	2.26	2.23	2.25	2.23	2.06	2.58	1.34	1.40	1.50[21]
LFlav-7	1.91	2.12	2.11	2.04	2.04	2.01	2.36	1.35	1.32	1.26[21]
Flav-7	1.90	2.06	2.05	1.95	1.95	1.94	2.25	1.29	1.24	1.21[21]
Flav-9	1.84	2.00	2.00	1.86	1.86	1.84	2.18	1.15	1.15	1.12[21]
MAE	0.51	0.80	0.77	0.81	0.79	1.16	0.69	0.09	0.06	
Naph.	4.27	4.57	4.49	4.93	4.78	4.62	5.11	4.23	4.06	4.10[27,28]
Anth.	3.15	3.53	3.44	4.17	4.01	3.68	4.13	3.35	3.34	3.26[29]
Tetra.	2.39	2.77	2.69	3.42	3.28	2.86	3.39	2.70	2.68	2.60[27,28]
Pyrene	3.52	3.86	3.78	4.32	4.17	4.07	4.47	3.17	3.16	3.38[19]
Penta.	1.83	2.17	2.11	2.79	2.68	3.17	2.74	2.32	2.45	2.14[30]
$C_{96}H_{24}$	1.44	1.82	1.74	2.53	2.39	2.81	2.69	1.90	2.01	2.00[31]
MAE	0.25	0.27	0.23	0.78	0.64	0.84	0.62	0.13	0.12	

experimental data. The upper panel illustrates the TDDFT results via the CAM-LDA0 functional, and the lower panel shows the TDHF@v_W (with parameterized v_W) spectra. The Flav-9 parameters are used again for ICG dye calculations, and the corannulene parameters are used for curved hydrocarbons. As expected, the more sophisticated treatment of the screening in the exchange kernel with v_W enables accurate prediction of the optical gaps. Therefore, it produces absorption peaks that are close to the experimental references (MAE < 0.1 eV).

Figure 5 shows the MAE of the optical gaps for all 20 systems studied in this work from various TDDFT/TDHF methods

with the experimental references. The TDHF@v_W (with parameterized v_W) achieves an MAE of 0.08 eV overall. In contrast, among all TDDFT functionals, TD-LDA produces an MAE of 0.45 eV, TD-PBE0: 0.55 eV, TD-B3LYP: 0.51 eV, TD-LC-PBE: 0.76 eV, TD-ωB97X: 0.68 eV, TD-CAM-LDA0: 0.68 eV, and TDHF: 1.01 eV.

More importantly, since one set of parameters works for a family of molecules and the parameters are grid-independent, the TDHF@v_W calculation here scales essentially the same as a typical TDDFT but with an updated and more sophisticated exchange kernel.
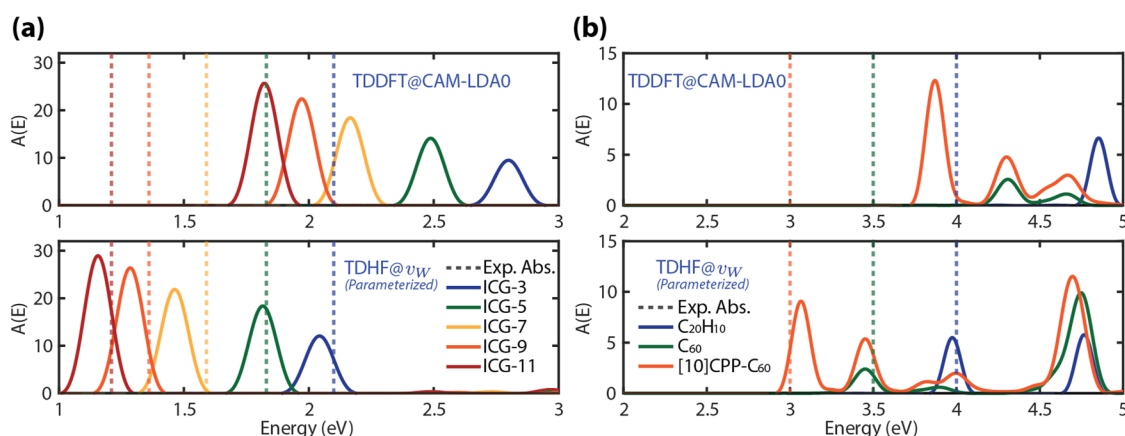
FIG. 4. Linear response absorption spectra using TDDFT@CAM-LDA0 (upper panel) and TDHF@v_W with parameterized v_W (lower panel) for (a) ICG dye family and (b) curved hydrocarbons ($C_{20}H_{10}$, C_{60}, and [10]CPP-C_{60}). Experimental excitation peaks are shown in dotted lines, ICG data are from Refs. 33–36, and curved hydrocarbons are from Refs. 20, 37, and 38.
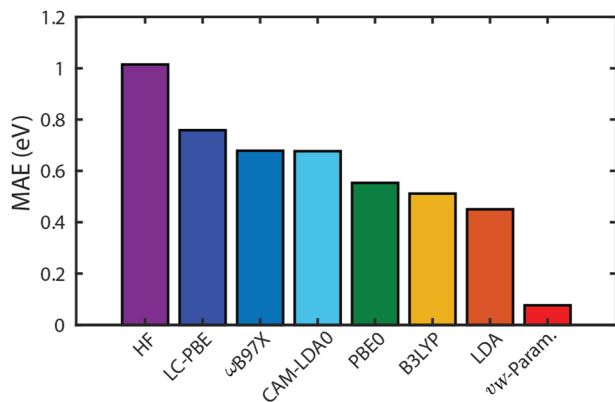
FIG. 5. MAE (in eV) of the optical gaps for 20 test molecules from various TDDFT/TDHF calculations against the experimental references.

IV. CONCLUSION

We introduce a parameterization scheme for the screened exchange kernel, v_W, which leverages the photophysical similarity among molecules within a given family (i.e., molecules that carry similar static dielectric responses) to bypass calculating and individually fitting the effective screened interaction, $W(r, r')$, for each molecule. Our approach provides a transferable, grid-independent kernel (with only seven parameters) derived from a compact parameterization of the inverse dielectric function, ϵ^{-1}. While chosen for mathematical convenience, our parameterization correctly reproduces on-site and asymptotic screening, ensuring physical fidelity. This method not only reduces computational overhead but also maintains accuracy in our TDHF@v_W spectral calculations.

We test this methodology across a diverse set of molecular systems, including π-conjugated polymethine cyanine dyes and planar and curved hydrocarbons. In each case, the S_1 excitation spectra show good agreement with results obtained from the individually fitted v_W while also aligning well with experimental reference values, yielding an MAE ~0.1 eV. This consistency highlights the robustness and transferability of our parameterized kernel approach. In addition, computational costs remain comparable to conventional TDHF or TDDFT with global or range-separated hybrid functionals while providing an improved treatment of electron–hole screening.

While we have demonstrated this approach with three specific parameterization sets, it lays the foundation for broader applications, allowing the development of a standardized library of parameters that can facilitate efficient and scalable excitation spectra predictions for increasingly large and complex systems. Given its balance between computational efficiency and accuracy, MBPT-based TDHF@v_W with a parameterized v_W represents another step toward achieving BSE-quality spectral calculations at the computational cost of traditional TDHF, further bridging the gap between accuracy and feasibility in excited-state simulations. As a future direction, self-consistently optimizing v_W could further improve the accuracy of our approach, in the spirit of the bootstrap procedure for the exchange–correlation kernel developed by Sharma *et al.*[39]

AUTHOR DECLARATIONS

Conflict of Interest

The authors have no conflicts to disclose.

Author Contributions

Barry Y. Li: Conceptualization (equal); Formal analysis (lead); Methodology (lead); Visualization (lead); Writing – original draft (lead); Writing – review & editing (equal). **Tim Duong**: Data curation (lead); Formal analysis (equal); Writing – original draft (equal); Writing – review & editing (equal). **Tucker Allen**: Methodology (equal); Validation (equal); Writing – original draft (equal); Writing – review & editing (equal). **Nadine C. Bradbury**: Methodology (equal); Software (equal); Writing – original draft (equal); Writing – review & editing (equal). **Justin R. Caram**: Funding acquisition (equal); Investigation (lead); Supervision (lead); Writing – review & editing (equal). **Daniel Neuhauser**: Conceptualization (lead); Funding acquisition (lead); Methodology (equal); Software (lead); Supervision (lead); Writing – review & editing (equal).

DATA AVAILABILITY

The data that support the findings of this study are available within the article and appendixes. Additional data, source codes, and tutorial videos that support the findings and reproducibility of this study are available from the corresponding author upon reasonable request.

APPENDIX A: HYDROCARBON STRUCTURES

Optimized hydrocarbon structures used in this study are shown in Fig. 6.

APPENDIX B: k_{mt} SENSITIVITY TEST

The spectral sensitivity with respect to k_{mt} is tested using pyrene; the result is shown in Fig. 7.
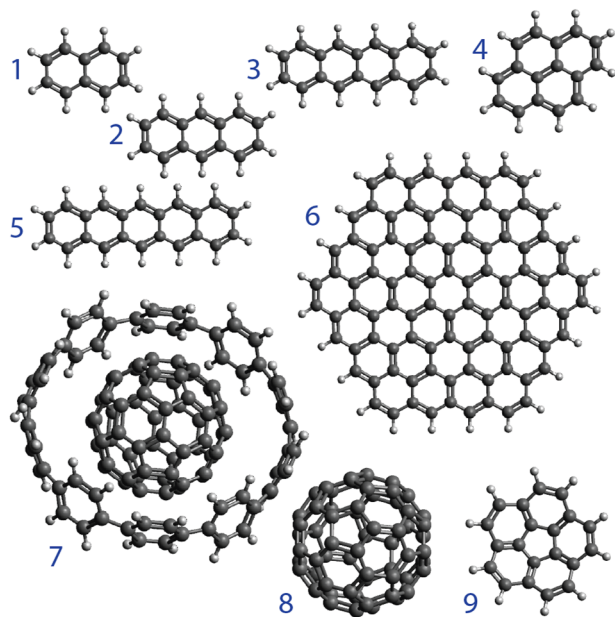
FIG. 6. Hydrocarbon systems tested in this work: (1) naphthalene (Naph.), (2) anthracene (Anth.), (3) tetracene (Tetra.), (4) pyrene, (5) pentacene (Penta.), (6) $C_{96}H_{24}$, (7) [10]CPP-C_{60}, (8) C_{60}, and (9) corannulene ($C_{20}H_{10}$).

APPENDIX C: COMPUTATION PARAMETERS

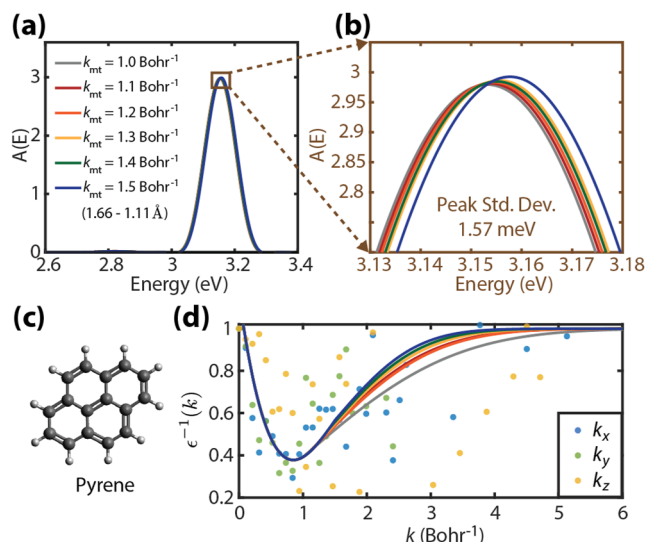General computational parameters for all systems are included in Table III.

FIG. 7. (a) S_1 excitation peak of pyrene calculated via TDHF@v_W with parameterized v_W at different k_{mt}. (b) Zoomed-in peak positions of (a); the standard deviation of the peak positions is 1.57 meV. (c) Molecular structure of pyrene. (d) $\epsilon^{-1}(k)$ parameterization with different k_{mt}; the color coding is the same as in (a).

TABLE III. Computational grids ($dr = dx = dy = dz$, unit: bohr), N_v, and N_c. $N_{k\text{-low}}$ is the number of deterministically treated long-wavelength terms, and the high-k space is represented with 1000 sparse stochastic vectors. Details can be found in Refs. 9 and 13.

| System	n_x	n_y	n_z	dr	N_v	N_c	$N_{k\text{-low}}$
ICG-3	110	100	80	0.4	105	400	953
ICG-5	120	100	80	0.4	110	400	1045
ICG-7	130	100	80	0.4	115	400	1127
ICG-9	130	100	80	0.4	120	400	1127
ICG-11	150	100	80	0.4	125	400	1293
Flav-1	100	100	80	0.4	96	400	867
Flav-3	110	100	80	0.4	101	400	953
Flav-5	140	100	80	0.4	106	400	1195
LFlav-7	140	100	80	0.4	111	400	1195
Flav-7	140	100	80	0.4	122	400	1195
Flav-9	120	120	120	0.5	116	400	3743
$C_{20}H_{10}$	60	60	60	0.5	45	185	461
C_{60}	60	60	60	0.5	120	400	461
[10]CPP-C_{60}	80	80	50	0.5	260	800	1551
Naph.	50	40	30	0.5	24	100	461
Anth.	60	40	30	0.5	33	100	739
Tetra.	70	40	30	0.5	42	150	1045
Pyrene	60	60	60	0.5	37	150	461
Penta.	80	40	30	0.5	51	200	1045
$C_{96}H_{24}$	100	100	30	0.5	204	650	2801
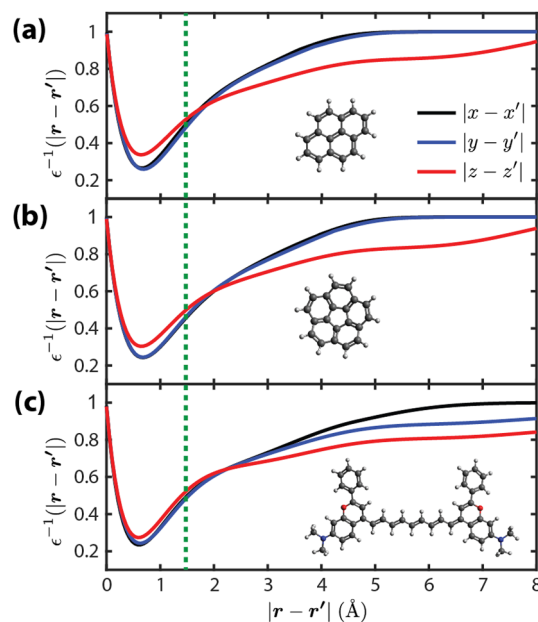
FIG. 8. Real-space inverse dielectric functions for (a) pyrene, (b) corannulene, and (c) Flav-9. The distances along the x, y, and z directions are plotted as $|x - x'|$, $|y - y'|$, and $|z - z'|$, respectively. The green dotted line indicates the typical C=C bond length ($\sim$1.4 Å) in conjugated systems.

APPENDIX D: REAL-SPACE REPRESENTATION OF $\epsilon^{-1}(|r - r'|)$

Real-space representations of the inverse dielectric function are illustrated in Fig. 8.

REFERENCES

[1] P. Boulanger, D. Jacquemin, I. Duchemin, and X. Blase, J. Chem. Theory Comput. **10**, 1212–1218 (2014).

[2] D. Jacquemin, I. Duchemin, and X. Blase, J. Phys. Chem. Lett. **8**, 1524–1529 (2017).

[3] B. Le Guennic and D. Jacquemin, Acc. Chem. Res. **48**, 530–537 (2015).

[4] D. Jacquemin, E. A. Perpète, G. E. Scuseria, I. Ciofini, and C. Adamo, J. Chem. Theory Comput. **4**, 123–135 (2007).

[5] E. Rabani, R. Baer, and D. Neuhauser, Phys. Rev. B **91**, 235302 (2015).

[6] N. C. Bradbury, T. Allen, M. Nguyen, K. Z. Ibrahim, and D. Neuhauser, J. Chem. Phys. **158**, 154104 (2023).

[7] T. Allen, M. Nguyen, and D. Neuhauser, J. Chem. Phys. **161**, 114116 (2024).

[8] J. W. Negele, Rev. Mod. Phys. **54**, 913 (1982).

[9] M. Sereda, T. Allen, N. C. Bradbury, K. Z. Ibrahim, and D. Neuhauser, J. Chem. Theory Comput. **20**, 4196–4204 (2024).

[10] M. Rohlfing and S. G. Louie, Phys. Rev. B **62**, 4927 (2000).

[11] V. Vlček, E. Rabani, and D. Neuhauser, Phys. Rev. Mater. **2**, 030801(R) (2018).

[12] N. C. Bradbury, M. Nguyen, J. R. Caram, and D. Neuhauser, J. Chem. Phys. **157**, 031104 (2022).

[13] N. C. Bradbury, T. Allen, M. Nguyen, and D. Neuhauser, J. Chem. Theory Comput. **19**, 9239–9247 (2023).

[14] N. C. Bradbury, B. Y. Li, T. Allen, J. R. Caram, and D. Neuhauser, J. Chem. Phys. **161**, 141101 (2024).

[15] J. Sun, J. Yang, and C. A. Ullrich, Phys. Rev. Res. **2**, 013091 (2020).

[16] F. Neese, F. Wennmohs, U. Becker, and C. Riplinger, J. Chem. Phys. **152**, 224108 (2020).

[17] F. Neese, Wiley Interdiscip. Rev.: Comput. Mol. Sci. **12**, e1606 (2022).

[18] G. J. Martyna and M. E. Tuckerman, J. Chem. Phys. **110**, 2810 (1999).

[19] I. S. K. Kerkines, I. D. Petsalakis, G. Theodorakopoulos, and W. Klopper, J. Chem. Phys. **131**, 224315 (2009).

[20] N. Pastukhova, L. M. Samos, L. Zoppi, E. Pavlica, J. Mathew, G. Bratina, J. S. Siegel, and K. K. Baldridge, RSC Adv. **7**, 45601 (2017).

[21] E. D. Cosco, J. R. Caram, O. T. Bruns, D. Franke, R. A. Day, E. P. Farr, M. G. Bawendi, and E. M. Sletten, Angew. Chem., Int. Ed. **56**, 13126–13129 (2017).

[22] C. A. McKeon, S. M. Hamed, F. Bruneval, and J. B. Neaton, J. Chem. Phys. **157**, 074103 (2022).

[23] T. Yanai, D. P. Tew, and N. C. Handy, Chem. Phys. Lett. **393**, 51–57 (2004).

[24] Y. Ma, M. Rohlfing, and C. Molteni, Phys. Rev. B **80**, 241405 (2009).

[25] M. A. Mosquera, C. H. Borca, M. A. Ratner, and G. C. Schatz, J. Phys. Chem. A **120**, 1605–1612 (2016).

[26] Y. Tawada, T. Tsuneda, S. Yanagisawa, T. Yanai, and K. Hirao, J. Chem. Phys. **120**, 8425–8433 (2004).

[27] J. C. S. Costa, R. J. S. Taveira, C. F. R. A. C. Lima, A. Mendes, and L. M. N. B. F. Santos, Opt. Mater. **58**, 51 (2016).

[28] A. Menon, J. A. H. Dreyer, J. W. Martin, J. Akroyd, J. Robertson, and M. Kraft, Phys. Chem. Chem. Phys. **21**, 16240 (2019).

[29] C. Jaramillo-González, R. Morales Cueto, and W. Rodríguez-Córdoba, in *Concepts of Mathematical Physics in Chemistry: A Tribute to Frank E. Harris—Part B*, Advances in Quantum Chemistry, edited by J. R. Sabin and R. Cabrera-Trujillo (Academic Press, 2016), Vol. 72, pp. 61–94.

[30] F. Anger, J. O. Ossó, U. Heinemeyer, K. Broch, R. Scholz, A. Gerlach, and F. Schreiber, J. Chem. Phys. **136**, 054701 (2012).

[31] T. Liu, C. Tonnelé, S. Zhao, L. Rondin, C. Elias, D. Medina-Lopez, H. Okuno, A. Narita, Y. Chassagneux, C. Voisin, S. Campidelli, D. Beljonne, and J.-S. Lauret, Nanoscale **14**, 3826 (2022).

[32] E. D. Cosco, A. L. Spearman, S. Ramakrishnan, J. G. P. Lingg, M. Saccomano, M. Pengshung, B. A. Arús, K. C. Y. Wong, S. Glasl, V. Ntziachristos, M. Warmer, R. R. McLaughlin, O. T. Bruns, and E. M. Sletten, Nat. Chem. **12**, 1123–1130 (2020).

[33] M. M. M. Swamy, Y. Murai, K. Monde, S. Tsuboi, A. K. Swamy, and T. Jin, ACS Appl. Mater. Interfaces **16**, 17253 (2024).

[34] H. Langhals, A. Varja, P. Laubichler, M. Kernt, K. Eibl, and C. Haritoglou, J. Med. Chem. **54**, 3903 (2011).

[35] R. S. Gamage and B. D. Smith, Chem. Biomed. Imaging **2**, 384 (2024).

[36] H. Heng, G. Song, X. Cai, J. Sun, K. Du, X. Zhang, X. Wang, F. Feng, and S. Wang, Angew. Chem., Int. Ed. **61**, e202203444 (2022).

[37] H. Yasumatsu, T. Kondow, H. Kitagawa, K. Tabayashi, and K. Shobatake, J. Chem. Phys. **104**, 899 (1996).

[38] Y. Xu, R. Kaur, B. Wang, M. B. Minameyer, S. Gsänger, B. Meyer, T. Drewello, D. M. Guldi, and M. von Delius, J. Am. Chem. Soc. **140**, 13413 (2018).

[39] S. Sharma, J. K. Dewhurst, A. Sanna, and E. K. U. Gross, Phys. Rev. Lett. **107**, 186401 (2011).